crystals

Article

Wafer-Scale Semipolar Micro-Pyramid Lighting-Emitting Diode Array

Shuo Zhang [1,2,3], Yan Yan [1,2,3], Tao Feng [1,2,3], Yue Yin [1,2,3], Fang Ren [1,2,3], Meng Liang [1,2,3], Chaoxing Wu [4,5], Xiaoyan Yi [1,2,3,*], Junxi Wang [1,2,3], Jinmin Li [1,2,3] and Zhiqiang Liu [1,2,3,*]

1 Research and Development Center for Solid State Lighting, Institute of Semiconductors, Chinese Academy of Sciences, Beijing 100083, China; zshuo@semi.ac.cn (S.Z.); yanyan19@semi.ac.cn (Y.Y.); ftao18@semi.ac.cn (T.F.); yinyue@semi.ac.cn (Y.Y.); rf@semi.ac.cn (F.R.); liangmeng@semi.ac.cn (M.L.); jxwang@red.semi.ac.cn (J.W.); jmli@red.semi.ac.cn (J.L.)
2 Center of Materials Science and Optoelectronics Engineering, University of Chinese Academy of Sciences, Beijing 100049, China
3 Beijing Engineering Research Center for the 3rd Generation Semiconductor Materials and Application, Beijing 100083, China
4 College of Physics and Information Engineering, Fuzhou University, Fuzhou 350108, China; chaoxing_wu@fzu.edu.cn
5 Fujian Science & Technology Innovation Laboratory for Optoelectronic Information of China, Fuzhou 350108, China
* Correspondence: spring@semi.ac.cn (X.Y.); lzq@semi.ac.cn (Z.L.)

Abstract: InGaN-based micro-structured light-emitting diodes (µLEDs) play a critical role in the field of full-color display. In this work, selected area growth (SAG) of a micro-pyramid LED array was performed on a 2-inch wafer-scale patterned SiO_2 template (periodicity: 4 µm diameter), by which a uniform periodic µLED array was achieved. The single-element pyramid-shaped LED exhibited 6 equivalent semipolar {1-101} planes and a size of about 5 µm, revealing a good crystalline quality with screw and edge dislocation densities of 8.27×10^7 and 4.49×10^8 cm^{-2}. Due to the stress–relaxation out of the SAG, the as-built compressive strain was reduced to 0.59 GPa. The µLED array demonstrated a stable emission, confirmed by a small variation of electroluminescence (EL) peak wavelength over a wide range of current density up to 44.89 A/cm^2, as well as tiny fluctuations (within 1.9 nm) in the EL full width at half maximum. The photoluminescence peak wavelength exhibits a good uniformity throughout the whole wafer with a discrete probability of only 0.25%.

Keywords: wafer-scale; selected area growth (SAG); pyramid µLED array; photoluminescence; electroluminescence

check for updates

Citation: Zhang, S.; Yan, Y.; Feng, T.; Yin, Y.; Ren, F.; Liang, M.; Wu, C.; Yi, X.; Wang, J.; Li, J.; et al. Wafer-Scale Semipolar Micro-Pyramid Lighting-Emitting Diode Array. *Crystals* **2021**, *11*, 686. https://doi.org/10.3390/cryst11060686

Academic Editor: Chinho Park

Received: 19 May 2021
Accepted: 12 June 2021
Published: 15 June 2021

1. Introduction

Over the past few years, nitride-based light-emitting diodes (LEDs) with chip size larger than 200 µm have been proven to be a great success in general lighting, outdoor displaying, display backlighting, and many other applications [1–3]. Recently, there has been excitement in the display industry about micro-structured LEDs (µLEDs) with a size smaller than 50 µm [4,5]. Compared with the traditional cathode ray tube (CRT) and liquid-crystal display (LCD), as well as emerging organic LED technologies, nitride-based µLEDs hold the promise of visually perfect displays with lower power consumption, enhanced speed, higher luminescence, and feasibility of 2D integration [5,6], emerging as great candidates for the next generation of display technology in the applications of high-end televisions, mobile phones, wearable display panels, augmented reality, and virtual reality [7,8]. Various types of nitride microstructures have been widely investigated, including waveguides, micro-disks, rings, pyramids, and nanowires [9–13].

However, there are still some challenges lying ahead to achieve nitride-based µLED display. First, the complicated transfer printing method is costly, which makes it difficult for mass production at present, and equally so for monolithic full-color displays [14–16]. Second, bulk defect-related Shockley–Read–Hall (SRH) recombination, a strong polarization effect in c-plane InGaN multiple quantum wells (MQWs), and severe sidewall leakage related to dangling bonds, contaminations, and ion damages induced by inductively coupled plasma (ICP) etching all severely reduce the external quantum efficiency of µLEDs [17–19]. Furthermore, the quantum-confined Stark effect (QCSE) caused by the internal polarization field in MQWs would bring serious wavelength shifts and instability of µLEDs at different injected currents [20], which would subsequently lead to the Mura effect on the application of µLED display. In this regard, InGaN-based semipolar LEDs hold the potential to solve the above problems, with advantages in terms of wide bandgap tunability [21], reduced QCSE effect, and good stability in the emission wavelength. Thus, a wafer-scale µLED array grown on the semipolar plane is expected to achieve large-area full-color displays. Except for its ability to grow nitrides on homo semipolar substrates, selected area growth (SAG) on c-plane sapphire substrates would also provide great opportunities to achieve semi-polar growth over a wide area [22,23]. In addition, it is particularly important to study the uniformity of the optoelectronic characteristics of wafer-scale µLEDs.

In this work, we prepared a 2-inch wafer-scale micro-pyramid LED array with an InGaN MQWs structure on semipolar {1-101} planes through metal-organic vapor deposition (MOCVD). The epitaxial µLED array was grown via SAG on a patterned SiO_2 template and the size of an individual µLED pixel was about 5 µm. The wafer-scale morphology of the as-fabricated epilayer was characterized. The crystalline quality and biaxial stress of the epilayer was also investigated. Finally, the results of the electrical properties indicated that these µLEDs could still work well at a current density of about 44.9 A/cm^2. The wafer-scale photoluminescence (PL) performance exhibited good uniformity throughout the whole 2-inch area with a discrete probability of only 0.25%. The full width at half maximum (FWHM) of electroluminescence (EL) fluctuated within a range of ±1.9 nm on the whole wafer. This work opens a feasible pathway for the growth of mass-produced micro-pyramid LEDs arrays for the application of full-color displays.

2. Materials and Methods

2.1. Template Preparation

An n-GaN film (5 µm) was deposited on a 2-inch c-plane sapphire wafer by MOCVD (Veeco, K465i), utilizing trimethylgallium (TMGa), NH_3, and Silane (SiH_4) as Ga, N precursor, and n-doped source, respectively. A 40 nm-thick SiO_2 layer was first deposited on n-GaN film by plasma-enhanced chemical vapor deposition (PECVD) with temperature at 300 °C, pressure at 600 mTorr, RF-power at 50 W, and SiH_4, He, N_2O, and N_2 flow of 500, 25, 1000, and 475 sccm respectively, followed by a patterning process to create an array of holes with a periodicity of 6 µm and a diameter of 4 µm by using contact lithography, and reactive ion etching (RIE) process with a mixture of CF_4/O_2 gases. The wafer-scale patterned SiO_2/n-GaN structure acted as a template to achieve the SAG of the µLED array.

2.2. Formation of Pyramid µLED Array

The pyramid µLED array was grown on the SiO_2/n-GaN structure by MOCVD. During the epitaxy process, trimethylindium (TMIn), trimethylaluminum (TMAl), and magnesocene (Cp_2Mg) were adopted as In, Al precursor, and p-doped source, respectively. The growth condition of the epitaxial structure in the MOCVD process is summarized in Table 1. Considering the chemical etching effect of hydrogen (H_2) on nitride, H_2 and nitrogen (N_2) mixed gases with a moderate flow of 20/125 standard liters per minute (slm) acted as the carrier gas to avoid the flat top of the nitride pyramid. For the following epitaxy, no GaN buffer layer was adopted. An n-GaN layer was directly grown on the prepared template at a high temperature of 1070 °C, with SiH_4 flow of 23.7 standard cubic centimeters per minute (sccm), TMGa flow of 328 sccm, and NH_3 flow of 50 slm, for about 30 min, followed by three-period InGaN/GaN shallow-well (SW) and shallow-barrier (SB) layers at a temperature of 860 °C. Afterward, four-period InGaN (10 nm)/GaN (3 nm)

MQWs were grown at 885 °C and 760 °C with NH_3 flow of 40 slm. Triethylgallium (TEGa) flows for the InGaN well and GaN barrier were 140 and 450 sccm. AlGaN/GaN electron barrier layer, p-GaN, and p-GaN contact layer were deposited subsequently at 950 °C, 950 °C, and 680 °C, respectively. In the final step, the p-GaN layer was in-situ annealed at 720 °C in an N_2 atmosphere in order to form good p-contacts.

Table 1. The growth condition of the epitaxial structure in the MOCVD process.

Step	Temperature (°C)	Time (min)	NH_3 (slm)	TMGa (sccm)	TEGa (sccm)	TMAl (sccm)	TMIn (sccm)	SiH_4 (sccm)	Cp_2Mg (sccm)
n-GaN	1070	30	50	328	/	/	/	23.7	/
InGaN/GaN SW/SB (LOOP 3)	860 860	4 2	40 40	/ /	218 172	/ /	570 /	/ /	/ /
InGaN/GaN QW/QB (LOOP 4)	760 885	4 8	40 40	/ /	140 450	/ /	500 /	/ /	/ /
AlGaN/GaN EBL (LOOP 10)	950 950	0.5 0.5	10 10	67 67	/ /	62 /	/ /	/ /	160 /
p-GaN	950	10	50	80	/	/	/	/	340
p-GaN CL	680	1.5	40	/	140	/	352	/	175

2.3. Characterization

The morphology of the as-fabricated pattern of the SiO_2 template was probed using an atomic force microscope (AFM) (D3100, Veeco, New York, NY, USA). The as-grown pyramid µLED array was characterized with scanning electron microscopy (SEM) (Hitachi, Tokyo, Japan) at a working voltage of 4.4 kV. The crystalline quality of the as-grown epilayers was analyzed through X-ray diffraction (XRD) (Bede D1, Bede, Durham, United Kingdom) with a Cu Kα radiation source at 40 kV voltage and 35 mA current. PL microscopy (Horiba, Kyoto, Japan) was performed with a 325 nm He-Cd laser as the excitation source at power of 50 mW and spatial resolution of 2µm. Raman (Horiba, Kyoto, Japan) measurement was performed by using a 532 nm linearly polarized laser as the excitation source. The signals were collected by a spectrometer with a grating groove density of 1200 g/mm and a focal length of 800 mm under a backscattering configuration. The microstructure of the pyramid LED was characterized with a transmission electron microscope (TEM) (JEM-F200, JEOL, Tokyo, Japan), which was equipped with an energy-dispersive X-ray spectroscopy (EDS) detector (JEOL, Tokyo, Japan). The electrical characteristics of the LED were analyzed by a source meter (Keithley 2400, Keithley, New York, NY, USA).

3. Results and Discussion

A randomly selected 3D AFM image over an area of 40 × 40 μm^2 of the as-fabricated 2-inch wafer-scale patterned SiO_2 layer (thickness of 40 nm) on n-GaN template revealed a pattern consisting of uniformly created periodical holes, in which the hole diameter was 4 µm and the period was 6 µm (see, Figure 1a). The depth variation curve along a row of the SiO_2 layer is shown in Figure S1. The uniform pattern is beneficial to the gas flow distribution in the reactor during the growth and thus promotes the uniformity of the nitride microstructures, especially for those on wafer-scale substrates. The utilization of n-GaN instead of sapphire as the template aimed to provide a high-quality growth front and an electron injection layer. The pyramid µLED array on the patterned SiO_2 layer is schematically shown in Figure 1b. The µLED structure was grown directly on the patterned template through SAG, benefiting from the neglected nitride nucleation on the SiO_2 mask. The typical morphology of a pyramid µLED array is observed from a 25°-tilted SEM image (magnification: 500×) in Figure 1c, from which it can be seen that the growth exhibited good uniformity and selectivity, as epitaxy only took place in the pattern openings. Additionally, all µLED structures showed a smooth-faceted identical pyramid structure with a hexagonal base and consistent crystalline orientations. From the cross-section and magnified SEM images in the inset of Figure 1c, 6 equivalent planes enclosed the pyramid, and the side facet was at a 61.8° angle to the (0002) plane of nitride, whereby it could be determined that the side planes belonged to the {1-101} facets. This is ascribed to the slower growth rate of {1-101} planes than that of (0002), and indicates that the semipolar planes {1-101} were energetically stable. Under this growth configuration, the (0002) facet gradually became extinct at the convex surface due to the faster growth rate with sufficient epitaxial time, and a self-limiting pyramid structure ultimately formed, in which the crystalline orientation can be identified in the SEM image as a single pyramid μLED. The typical base size of the pyramid μLED was about 5 μm.

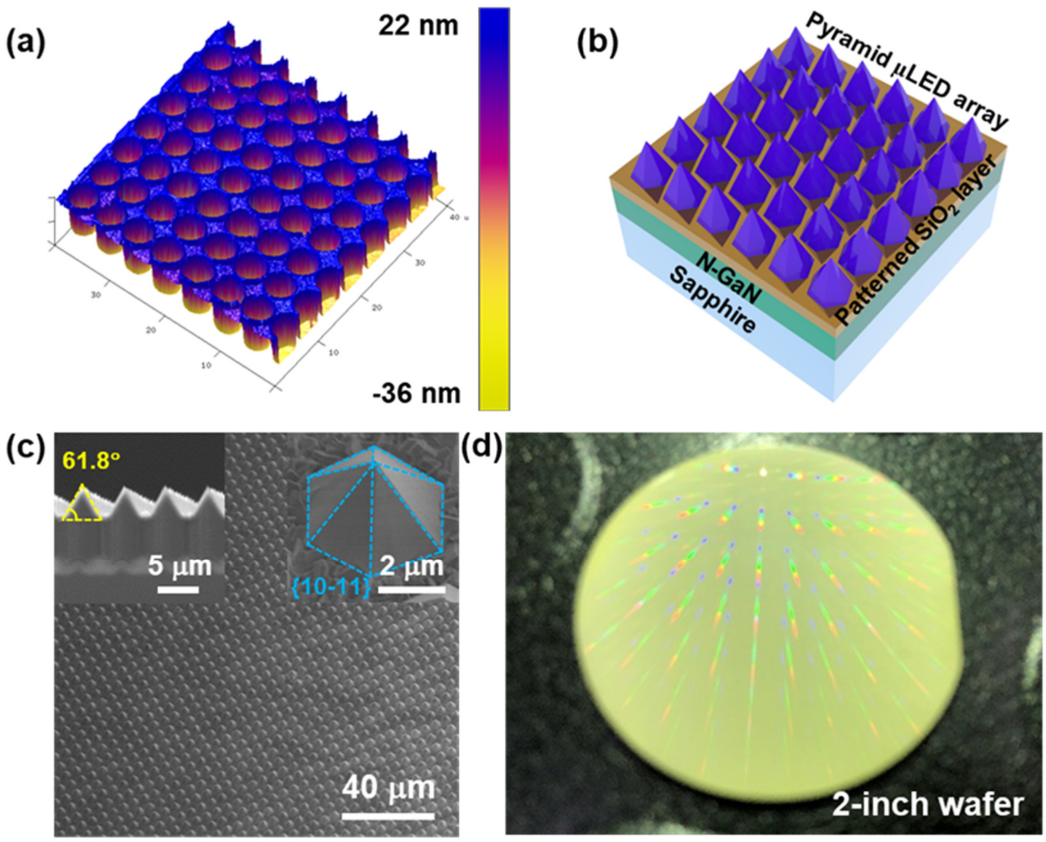

Figure 1. (**a**) AFM image of the as-fabricated patterned SiO_2 layer on n-GaN template; (**b**) Schematic diagram of the as-grown pyramid μLED array on patterned SiO_2 layer; (**c**) The 25° tilted SEM image (magnification: 500×) of the as-grown pyramid μLED array. The insets represent the cross-section SEM image and a magnified pyramid structure; (**d**) Photograph of the 2-inch wafer with pyramid μLED array.

An optical photograph of the as-fabricated wafer was obtained (see Figure 1d). Rainbow colors could be seen when white light was scattered by the complex periodic structure. It is observed that the rainbow color stripes covered the entire wafer, indicating the good uniformity and strong periodicity of the pyramid μLED array on the wafer.

To evaluate the crystalline quality of as-grown nitride, the FWHM of (0002) and (10-12) planes was measured as 202.9 and 247.9 arcsec, respectively (see Figure 2a). The screw and edge dislocation densities of nitride could be estimated according to the following equations [24]:

$$N_{screw} = \beta_{tilt}^2 / 4.35 b_s^2 \tag{1}$$

$$N_{edge} = \beta_{twist}^2 / 4.35 b_e^2 \tag{2}$$

where b_s and b_e are the Burgers vectors of the screw dislocation ($|b_s| = 0.5185$ nm for GaN) and edge dislocation ($|b_e| = 0.3189$ nm for GaN). β_{tilt} and β_{twist} are the tilt and twist spreads, respectively, which could be estimated by Equation (3) based on a previous report [25]:

$$\beta = \sqrt{(\beta_{tilt} \cos \varphi)^2 + (\beta_{twist} \sin \varphi)^2} \quad (3)$$

where φ is the angle between the reciprocal lattice vector (K_{hkl}) and the (001) plane normal. As such, the corresponding screw and edge dislocation densities of the as-grown epilayer were estimated as 8.27×10^7 and 4.49×10^8 cm^{-2}, respectively, indicating the good crystalline quality of the as-grown pyramid µLED layer.

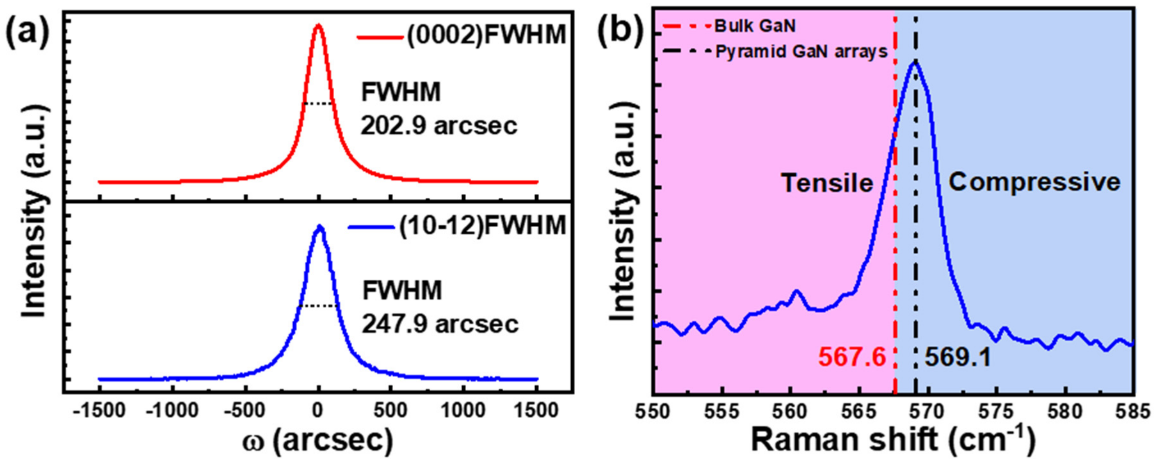

Figure 2. (**a**) XRD (0002) and (10-12) rocking curves, and (**b**) Raman spectrum of the as-grown pyramid µLED epitaxial structure on patterned SiO_2 layer.

Raman spectroscopy was performed to quantitatively investigate the stress of the as-grown µLED structure. The E_2 (high) peak mode in the Raman spectrum was closely related to the biaxial stress in the GaN film [26]. The peak position of the pyramid µLED structure was measured as 569.1 cm^{-1}, which deviates from the characteristic frequency of stress-free GaN (567.6 cm^{-1}) [27]. The biaxial stress σ_{xx} in the as-grown nitride layer could be estimated according to its frequency deviation $\Delta\omega$ compared with the stress-free GaN and the equation $\Delta\omega = K\sigma_{xx}$, where K is the linear stress coefficient of GaN material (2.56 cm^{-1}GPa^{-1}) [28]. Through calculation, the biaxial stress of µLED structure was identified as 0.59 GPa, meaning that the epilayer was subjected to a weak compressive strain, which benefited from micro-scale footprints of epilayer on the n-GaN template and the suppression of stress accumulations.

Detailed structural analysis of a single µLED pyramid in the array was characterized by TEM. The test lamella was fabricated using a focused ion beam. From the TEM image of a single pyramid µLED structure (see Figure 3a), a triangular outline is clearly resolved, corresponding to the cross-section of the pyramid. The SiO_2 pattern and the opening hole could be clearly identified at the bottom of the pyramid. The top of the pyramid was sharp and the angle between the sidewall and the in-plane was around 61.5°–62°, which is consistent with the above SEM result. Figure 3b shows the high-resolution TEM (HRTEM) image from the place of interest marked by a yellow square in Figure 3a. From selected area electron diffraction (SAED) patterns in the set of Figure 3b, the d-spacing along growth direction was calculated as 5.46 Å, corresponding to the (0002) plane of GaN, confirming the wurtzite structure of epilayer, [0001] growth direction of epilayer, and <10-11> equivalent orientation perpendicular to the sidewall of the pyramid. Cross-section high angle annular dark-field (HAADF) scanning transmission electron microscopy (STEM) and corresponding EDS mapping of In from region B in Figure 3a were performed to evaluate the structure of MQWs, due to their good sensitivity and contrast to elements with different atomic numbers (see Figure 3c,d). The results indicate that three-period InGaN/GaN shallow quantum well and four-period InGaN/GaN MQWs exhibited obvious light and dark stripes. The separate dark stripe near the sidewall represented the AlGaN electron barrier layer, aiming to block the electron roll-over effect under the operation of high current density and further reduce the probability of electron-hole pair non-radiative recombination.

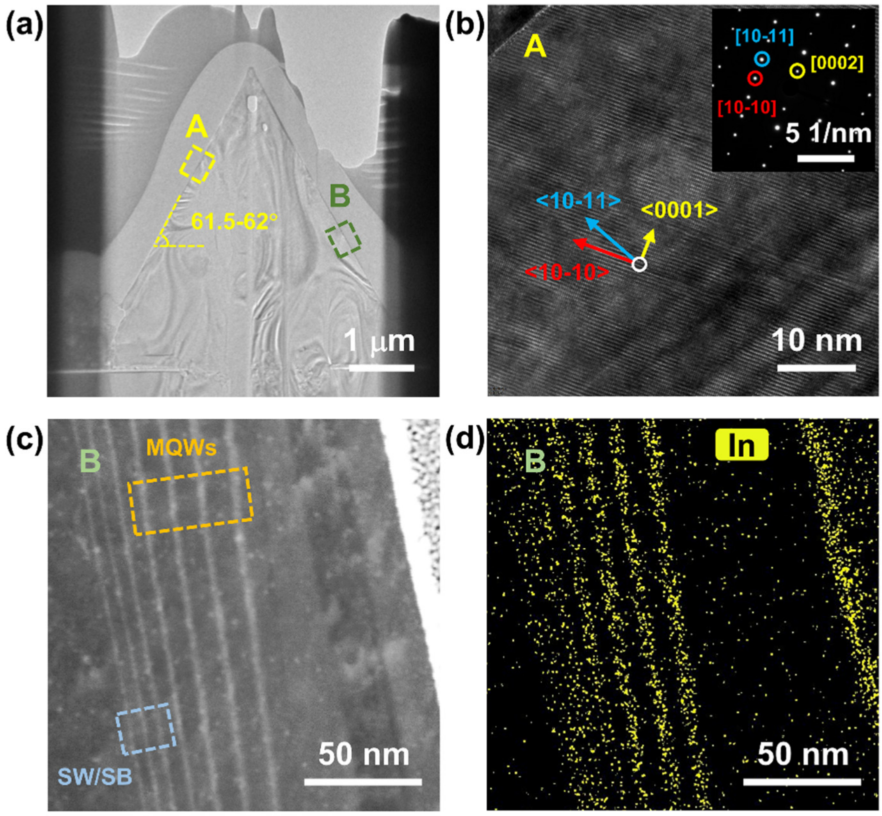

Figure 3. (**a**) TEM image of a single pyramid μLED structure; (**b**) HRTEM image of region A in (**a**), including part of the MQWs structure and the p-GaN layer; inset is the image of corresponding SAED patterns; (**c**) HAADF STEM image of region B in (**a**), including MQWs and p-GaN layer in the μLED structure; (**d**) EDS mapping of In element in MQWs, corresponding to (**c**).

The electrical characteristics of the as-fabricated wafer-scale pyramid μLED array were investigated by on-wafer electrical probing. Indium bumps were pinned on the wafer, serving as n-type and p-type contacts, respectively, while the n-GaN template acted as the n-type current spreading layer. The injected current density depends on the size of the indium bumps on the surface of the wafer (approximately 1 mm^2 in this work). The I-V characteristic of the μLED array demonstrated a good rectification characteristic with a threshold voltage of 4.13 V (defined as the voltage value at an injection current of 1 mA) (see Figure 4a), which was slightly larger than that of conventional μLED chips. To explore the reason for this, the parasitic resistance characteristic of the μLED array was analyzed. The series resistance is generally influenced by various resistances including p-type contacts, n-type contacts, and especially the intrinsic resistance of the n-GaN layer in this work, as n-contacts were far away from the devices. Linear fitting of IdV/dI and I in the moderate current region (4–18 mA) showed that the series resistance of μLED array was calculated as 223.1 Ω (see Figure S2) [29]. The parallel resistance is normally related to the damage on MQWs and the surface defects of the epilayer, leading to a bypass current vertically through the LED structure. The parallel resistance was estimated to be 610 kΩ through the linear fitting of the I-V curve within the low voltage region (0–2.5 V), indicating the good crystalline quality of the epilayer (see Figure S3).

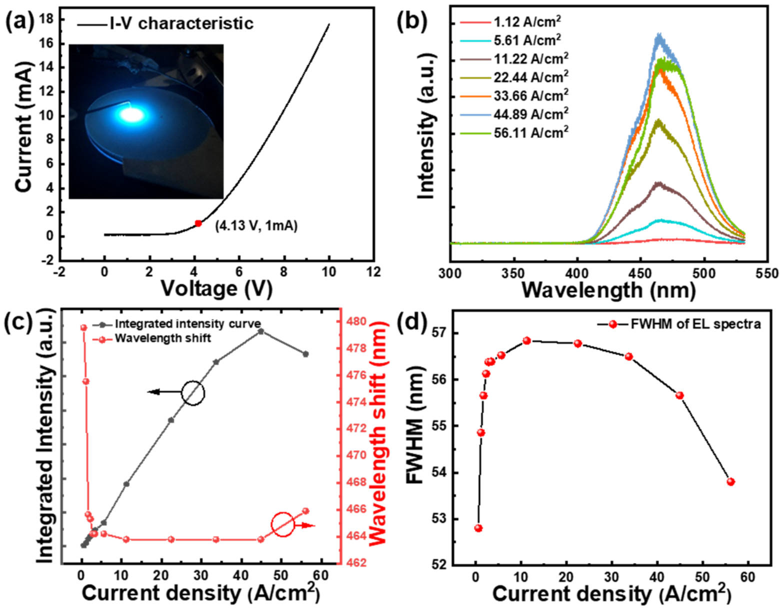

Figure 4. (**a**) The I-V characteristic of wafer-scale pyramid µLED array measured through on-wafer electrical probing; the inset is a photograph of the LED operated at 22.44 A/cm^2; (**b**) EL spectra of the wafer-scale pyramid µLED array as a function of injected current density; (**c**) the integrated EL intensity and wavelength peak shift curve as a function of injected current density; (**d**) the FWHM of EL spectra as a function of injected current density.

The electrical luminescence picture from the µLED array in the inset of Figure 4a exhibited a uniform blue light emission on the wafer. The EL spectral spectra of the µLED array at different injected current densities (from 1.12 to 56.11 A/cm^2) were also collected (Figure 4b). The EL peak position and EL integrated intensity as a function of injected current densities are summarized in Figure 4c. As the current density increased, the EL peaks first blue-shifted about 16 nm (current density from 1.12 to 11.22 A/cm^2), then maintained stability at 463.8 nm in a wide range (current density from 11.22 to 44.89 A/cm^2), and eventually exhibited a redshift of about 2.1 nm (current density from 44.89 to 56.11 A/cm^2). The large blue shift could be largely attributed to different active regions, which have various strain states, to In atoms in the localized regions, or to the MQWs structure on (0002) plane [30,31]. In addition, the screening of charge to the built-in electrical field within the MQWs and the band filling effect as injected current density increased could also lead to a reduction in QCSE for the emission wavelength [32]. The bandgap of semiconductors decreases with increasing temperatures when self-heating effects start to take over at a high injected current density of LED, which causes redshift in the LED emission wavelength [33]. The EL integrated intensity increased first in a large current density range of 1.12–44.89 A/cm^2 and then decreased [34]. This is presumably attributed to the electrical breakdown of individual pyramid µLEDs at high current densities. As shown in Figure 4d, weak fluctuations centered at 56 nm FWHM of pyramid µLED array were observed. The wide EL spectrum is due to the native fluctuation of indium composition in the InGaN layer and the uneven thickness of the quantum well deposited on the semipolar plane of nitride [31,35]. The FWHM reached a maximum when the operating current density was 11.22 A/cm^2.

In this section, to investigate the uniformity of optical properties of wafer-scale pyramid µLED, we adopted the standard frequency distribution histogram for summarizing the PL peak wavelength data based on 40 samples (Figure 5a). The 40 samples are located on the 2-inch wafer, labeled as "1–40" (Figure 5b). The minimum and maximum were 490.85 and 495.57 nm, respectively. The fluctuation range of the PL wavelength peak within the 2-inch wafer-scale was less than 5 nm, indicating the preferable uniformity of the peak wavelength distribution. This helps to fabricate a large-scale µLED array with the same luminous characteristics. Additionally, more than half of the samples had peak wavelengths within the range of 490.7 to 492 nm. The standard deviation (Std. Dev.) was derived as 1.22 nm, and the relative Std. Dev. (defined as Std. Dev./mean × 100%) was calculated as 0.25%. This means that the discrete probability of PL peak wavelength was only 0.25%, proving that the pyramid µLED array had uniform optical properties throughout the whole 2-inch wafer.

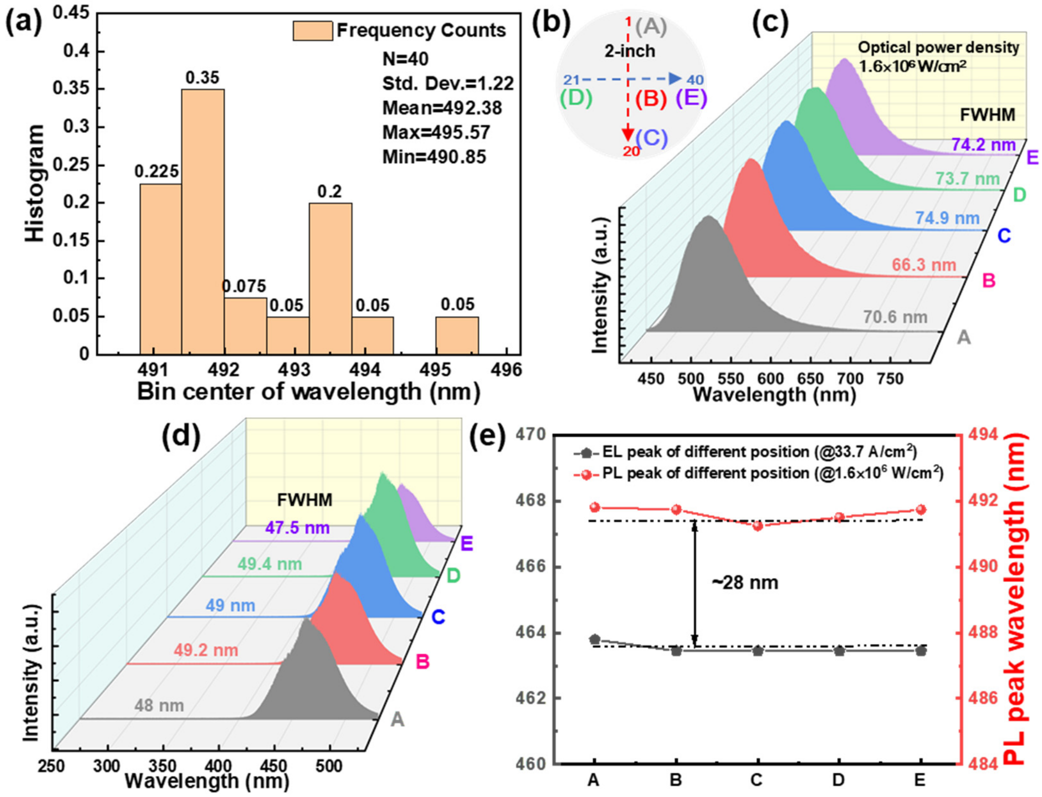

Figure 5. (**a**) The standard frequency distribution histogram of the PL peak wavelength. Number of samples (N) is 40; (**b**) Schematic diagram of locations of interests for PL spectroscopy, among which labels "1–40" represent the samples and labels "A–E" represent five samples with representative characteristics; (**c**) PL spectra (at an optical power density of 1.6×10^6 W/cm^2) and (**d**) EL spectra (at injected current density of 33.7 A/cm^2) of the five samples; (**e**) EL and PL peak wavelengths of the five samples at different positions.

To illustrate detailed spectra characteristics, we selected five samples with representative characteristics and compared their PL and EL spectra (Figure 5c–e). The optical power density of the excited light source in the PL measurement remained steady at 1.6×10^6 W/cm^2, and EL spectra were collected at the injected current density of 33.7 A/cm^2. The PL FWHM fluctuated in a range of ±8.6 nm, which is attributed to the generation of localization centers [31]. As shown in Figure 5c,d, the value of the EL FWHM was on average 28 nm smaller than that of the PL and had smaller fluctuations within ±1.9 nm, indicating that some localization centers are not electrically excited under conditions of certain current density. Additionally, as shown in Figure 5e, the peak wavelength of EL fluctuated within only ±0.34 nm. A uniform EL characteristic is helpful to the stability of LED devices. The comparison of PL and EL peak wavelengths was also summarized. The mean PL peak wavelength demonstrated an obvious redshift of about 28 nm more than the EL peak wavelength, which may be related to Stokes' shift induced by indium composition fluctuations in the PL measurement and the band filling effect in the EL measurement [36]. Moreover, the higher junction temperature in optical injection mode than in current injection mode may also be an important factor, which could be explained by the thermal emission of the illuminating laser [37].

4. Conclusions

In summary, a micro-pyramid LED array was fabricated on an entire 2-inch sapphire wafer through the SAG method by MOCVD. The μLED pixels in the array were of the size of about 5 μm, exhibiting excellent uniformity in size and morphology. Meanwhile, good crystalline quality with weak compressive strain was confirmed by XRD and Raman spectroscopy for the LED epitaxial layers. Furthermore, the μLED array showed a wafer-scale uniformity of optoelectronic characteristics through wafer-coverage PL and EL measurements. The peak wavelength and FWHM of EL fluctuations were within only 1.9 and 0.34 nm, respectively, demonstrating very stable EL emission properties. The discrete probability of PL peak wavelength throughout the whole 2-inch wafer was only 0.25%. Since the InGaN-based micro-pyramid LED array has such stable and uniform optoelectronic performance, the strategy proposed in this work can likely be used to achieve the fabrication of full-color display units. Future work can be conducted to study the multiple SAG of InGaN-based pyramid LED arrays with different emission wavelengths to achieve on-chip integration of the three primary colors.

Supplementary Materials: The following are available online at https://www.mdpi.com/article/10.3390/cryst11060686/s1, Figure S1: The linear fitting result of the IdV/dI curve as a function of I in the moderate current region (4–18 mA), Figure S2: The linear fitting result of the IdV/dI curve as a function of I in the moderate current region (4–18 mA), Figure S3: The linear fitting result of the I-V curve in the low voltage region (0–2.5 V) of the as-fabricated LED.

Author Contributions: S.Z. and Y.Y. (Yan Yan) contributed equally to this work. Design and execution of experiments, S.Z. and Y.Y. (Yan Yan); formal analysis, S.Z. and Y.Y. (Yan Yan); supervision and discussion of results, T.F., Y.Y. (Yue Yin), F.R., M.L., and C.W.; validation, S.Z. and Y.Y. (Yan Yan); writing—original draft preparation, S.Z. and Y.Y. (Yan Yan); writing—review and editing, S.Z., Y.Y. (Yan Yan), X.Y., J.W., J.L., Z.L.; project administration, X.Y., J.W., J.L., Z.L.; funding acquisition, X.Y. and Z.L. All authors have read and agreed to the published version of the manuscript.

Funding: This research was funded by the National Key R&D Program of China (Grant Nos. 2017YFB0403100 and 2017YFB0403103) and the National Natural Science Foundation of China (Grant Nos. 61974140 and 61604140).

Data Availability Statement: The data that support the findings of this study are available from the corresponding author upon reasonable request.

Conflicts of Interest: The authors declare no conflict of interest.

References

1. Tan, G.; Huang, Y.; Li, M.C.; Lee, S.L.; Wu, S.T. High dynamic range liquid crystal displays with a mini-LED backlight. *Opt. Express* **2018**, *26*, 16572–16584. [CrossRef]
2. Kim, K.; Hua, M.; Liu, D.; Kim, J.; Chen, K.J.; Ma, Z. Efficiency enhancement of InGaN/GaN blue light-emitting diodes with top surface deposition of AlN/Al2O3. *Nano Energy* **2018**, *43*, 259–269. [CrossRef]
3. Wu, T.; Lin, Y.; Zhu, H.; Guo, Z.; Zheng, L.; Lu, Y.; Shih, T.M.; Chen, Z. Multi-function indoor light sources based on light-emitting diodes-a solution for healthy lighting. *Opt. Express* **2016**, *24*, 24401–24412. [CrossRef]
4. Jin, S.X.; Shakya, J.; Lin, J.Y.; Jiang, H.X. Size dependence of III-nitride microdisk light-emitting diode characteristics. *Appl. Phys. Lett.* **2001**, *78*, 3532–3534. [CrossRef]
5. Zhang, K.; Peng, D.; Lau, K.M.; Liu, Z. Fully-integrated active matrix programmable UV and blue micro-LED display system-on-panel (SoP). *J. Soc. Inf. Disp.* **2017**, *25*, 240–248. [CrossRef]
6. Iga, K. Forty years of vertical-cavity surface-emitting laser: Invention and innovation. *Jpn. J. Appl. Phys.* **2018**, *57*, 08PA01. [CrossRef]
7. Jiang, H.X.; Lin, J.Y. Nitride micro-LEDs and beyond–A decade progress review. *Opt. Express* **2013**, *21* (Suppl. 3), A475–A484. [CrossRef]
8. Lin, J.Y.; Jiang, H.X. Development of microLED. *Appl. Phys. Lett.* **2020**, *116*, 100502. [CrossRef]
9. Tabataba-Vakili, F.; Brimont, C.; Alloing, B.; Damilano, B.; Doyennette, L.; Guillet, T.; el Kurdi, M.; Chenot, S.; Brändli, V.; Frayssinet, E.; et al. Analysis of low-threshold optically pumped III-nitride microdisk lasers. *Appl. Phys. Lett.* **2020**, *117*, 121103. [CrossRef]
10. Makela, M.; Gordon, P.; Tu, D.; Soliman, C.; Cote, G.L.; Maitland, K.; Lin, P.T. Benzene Derivatives Analysis Using Aluminum Nitride Waveguide Raman Sensors. *Anal. Chem.* **2020**, *92*, 8917–8922. [CrossRef]

11. Lu, T.J.; Fanto, M.; Choi, H.; Thomas, P.; Steidle, J.; Mouradian, S.; Kong, W.; Zhu, D.; Moon, H.; Berggren, K.; et al. Aluminum nitride integrated photonics platform for the ultraviolet to visible spectrum. *Opt. Express* **2018**, *26*, 11147–11160. [CrossRef] [PubMed]
12. Choi, J.H.; Zoulkarneev, A.; Kim, S.I.; Baik, C.W.; Yang, M.H.; Park, S.S.; Suh, H.; Kim, U.J.; Son, H.B.; Lee, J.S.; et al. Nearly single-crystalline GaN light-emitting diodes on amorphous glass substrates. *Nature Photonics* **2011**, *5*, 763–769. [CrossRef]
13. Zhang, S.; Zhang, X.; Ren, F.; Yin, Y.; Feng, T.; Song, W.; Wang, G.; Liang, M.; Xu, J.; Wang, J.; et al. High responsivity GaN nanowire UVA photodetector synthesized by hydride vapor phase epitaxy. *J. Appl. Phys.* **2020**, *128*, 155705. [CrossRef]
14. Zhang, L.; Ou, F.; Chong, W.C.; Chen, Y.; Li, Q. Wafer-scale monolithic hybrid integration of Si-based IC and III-V epi-layers-A mass manufacturable approach for active matrix micro-LED micro-displays. *J. Soc. Inf. Disp.* **2018**, *26*, 137–145. [CrossRef]
15. Zhuang, Z.; Guo, X.; Liu, B.; Hu, F.; Li, Y.; Tao, T.; Dai, J.; Zhi, T.; Xie, Z.; Chen, P.; et al. High Color Rendering Index Hybrid III-Nitride/Nanocrystals White Light-Emitting Diodes. *Adv. Funct. Mater.* **2016**, *26*, 36–43. [CrossRef]
16. Chen, Z.; Yan, S.; Danesh, C. MicroLED technologies and applications: Characteristics, fabrication, progress, and challenges. *J. Phys. D Appl. Phys.* **2021**, *54*, 123001. [CrossRef]
17. Olivier, F.; Tirano, S.; Dupré, L.; Aventurier, B.; Largeron, C.; Templier, F. Influence of size-reduction on the performances of GaN-based micro-LEDs for display application. *J. Lumin.* **2017**, *191*, 112–116. [CrossRef]
18. Tian, P.; McKendry, J.J.D.; Gong, Z.; Guilhabert, B.; Watson, I.M.; Gu, E.; Chen, Z.; Zhang, G.; Dawson, M.D. Size-dependent efficiency and efficiency droop of blue InGaN micro-light emitting diodes. *Appl. Phys. Lett.* **2012**, *101*, 231110. [CrossRef]
19. Wong, M.S.; Hwang, D.; Alhassan, A.I.; Lee, C.; Ley, R.; Nakamura, S.; DenBaars, S.P. High efficiency of III-nitride micro-light-emitting diodes by sidewall passivation using atomic layer deposition. *Opt. Express* **2018**, *26*, 21324–21331. [CrossRef] [PubMed]
20. Craven, M.D.; Lim, S.H.; Wu, F.; Speck, J.S.; DenBaars, S.P. Structural characterization of nonpolar (112¯0) a-plane GaN thin films grown on (11¯02) r-plane sapphire. *Appl. Phys. Lett.* **2002**, *81*, 469–471. [CrossRef]
21. Northrup, J.E. GaN and InGaN(1122) surfaces: Group-III adlayers and indium incorporation. *Appl. Phys. Lett.* **2009**, *95*, 133107. [CrossRef]
22. Ahmed, R.; Siddique, A.; Anderson, J.; Gautam, C.; Holtz, M.; Piner, E. Integration of GaN and Diamond Using Epitaxial Lateral Overgrowth. *ACS Appl. Mater. Interfaces* **2020**, *12*, 39397–39404. [CrossRef] [PubMed]
23. Wernicke, T.; Schade, L.; Netzel, C.; Rass, J.; Hoffmann, V.; Ploch, S.; Knauer, A.; Weyers, M.; Schwarz, U.; Kneissl, M. Indium incorporation and emission wavelength of polar, nonpolar and semipolar InGaN quantum wells. *Semicond. Sci. Technol.* **2012**, *27*, 27. [CrossRef]
24. Ni, R.; Chen, X.; Yan, J.; Zhang, L.; Guo, Y.; Wang, J.; Li, J.; Zhang, Y. Reducing stimulated emission threshold power density of AlGaN/AlN multiple quantum wells by nano-trench-patterned AlN template. *J. Alloys Compd.* **2019**, *777*, 344–349. [CrossRef]
25. Lee, S.R.; West, A.M.; Allerman, A.A.; Waldrip, K.E.; Follstaedt, D.M.; Provencio, P.P.; Koleske, D.D.; Abernathy, C.R. Effect of threading dislocations on the Bragg peakwidths of GaN, AlGaN, and AlN heterolayers. *Appl. Phys. Lett.* **2005**, *86*, 241904. [CrossRef]
26. Zhang, S.; Liu, B.; Ren, F.; Yin, Y.; Wang, Y.; Chen, Z.; Jiang, B.; Liu, B.; Liu, Z.; Sun, J.; et al. Graphene-Nanorod Enhanced Quasi-Van Der Waals Epitaxy for High Indium Composition Nitride Films. *Small* **2021**, *17*, e2100098. [CrossRef]
27. Muhammed, M.M.; Roldan, M.A.; Yamashita, Y.; Sahonta, S.L.; Ajia, I.A.; Iizuka, K.; Kuramata, A.; Humphreys, C.J.; Roqan, I.S. High-quality III-nitride films on conductive, transparent (201)-oriented beta-Ga_2O_3 using a GaN buffer layer. *Sci. Rep.* **2016**, *6*, 29747. [CrossRef]
28. Park, A.H.; Seo, T.H.; Chandramohan, S.; Lee, G.H.; Min, K.H.; Lee, S.; Kim, M.J.; Hwang, Y.G.; Suh, E.K. Efficient stress-relaxation in InGaN/GaN light-emitting diodes using carbon nanotubes. *Nanoscale* **2015**, *7*, 15099–15105. [CrossRef]
29. Huang, H.-W.; Kao, C.C.; Chu, J.T.; Kuo, H.C.; Wang, S.C.; Yu, C.C. Improvement of InGaN-GaN light-emitting diode performance with a nano-roughened p-GaN surface. *IPTL* **2005**, *17*, 983–985. [CrossRef]
30. Gîrgel, I.; Edwards, P.R.; le Boulbar, E.; Coulon, P.-M.; Sahonta, S.-L.; Allsopp, D.W.E.; Martin, R.W.; Humphreys, C.J.; Shields, P.A. Investigation of indium gallium nitride facet-dependent nonpolar growth rates and composition for core–shell light-emitting diodes. *J. Nanophotonics* **2016**, *10*, 16010. [CrossRef]
31. Bi, Z.; Gustafsson, A.; Lenrick, F.; Lindgren, D.; Hultin, O.; Wallenberg, L.R.; Ohlsson, B.J.; Monemar, B.; Samuelson, L. High In-content InGaN nano-pyramids: Tuning crystal homogeneity by optimized nucleation of GaN seeds. *J. Appl. Phys.* **2018**, *123*, 25102. [CrossRef]
32. Senawiratne, J.; Chatterjee, A.; Detchprohm, T.; Zhao, W.; Li, Y.; Zhu, M.; Xia, Y.; Li, X.; Plawsky, J.; Wetzel, C. Junction temperature, spectral shift, and efficiency in GaInN-based blue and green light emitting diodes. *Thin Solid Films* **2010**, *518*, 1732–1736. [CrossRef]
33. Brown, I.H.; Pope, I.A.; Smowton, P.M.; Blood, P.; Thomson, J.D.; Chow, W.W.; Bour, D.P.; Kneissl, M. Determination of the piezoelectric field in InGaN quantum wells. *Appl. Phys. Lett.* **2005**, *86*, 131108. [CrossRef]
34. Liu, Z.; Wei, T.; Guo, E.; Yi, X.; Wang, L.; Wang, J.; Wang, G.; Shi, Y.; Ferguson, I.; Li, J. Efficiency droop in InGaN/GaN multiple-quantum-well blue light-emitting diodes grown on free-standing GaN substrate. *Appl. Phys. Lett.* **2011**, *99*, 91104. [CrossRef]
35. Griffiths, J.T.; Oehler, F.; Tang, F.; Zhang, S.; Fu, W.Y.; Zhu, T.; Findlay, S.D.; Zheng, C.; Etheridge, J.; Martin, T.L.; et al. The microstructure of non-polar a-plane (11 2¯0) InGaN quantum wells. *J. Appl. Phys.* **2016**, *119*, 175703. [CrossRef]

36. de Mierry, P.; Guehne, T.; Nemoz, M.; Chenot, S.; Beraudo, E.; Nataf, G. Comparison between Polar (0001) and Semipolar (11\bar22) Nitride Blue–Green Light-Emitting Diodes Grown onc- andm-Plane Sapphire Substrates. *Jpn. J. Appl. Phys.* **2009**, *48*, 48. [CrossRef]
37. Li, L.; Li, P.; Wen, Y.; Wen, J.; Zhu, Y. Temperature dependences of photoluminescence and electroluminescence spectra in light-emitting diodes. *Appl. Phys. Lett.* **2009**, *94*, 261103. [CrossRef]